Journal of Materials Chemistry A

Thermoelectric Properties of High-Performance n-Type Lead Telluride Measured In Situ in a Nuclear Reactor Core

Journal:	*Journal of Materials Chemistry A*
Manuscript ID	TA-COM-06-2022-004409.R1
Article Type:	Communication
Date Submitted by the Author:	16-Sep-2022
Complete List of Authors:	Kempf, Nicholas; University of Notre Dame, Aerospace and Mechanical Engineering Luo, Zhong-zhen; Northwestern University, Department of Chemistry Xie, Hongyao; Northwestern University Daw, Joshua; Idaho National Laboratory, Measurement Sciences Laboratory Kanatzidis, Mercouri; Northwestern University, Department of Chemistry Zhang, Yanliang; University of Notre dame, Department of Aerospace and Mechanical Engineering

Thermoelectric Properties of High-Performance n-Type Lead Telluride Measured In Situ in a Nuclear Reactor Core

Nicholas Kempf,[a] Zhong-Zhen Luo,[b] Hongyao Xie,[b] Joshua Daw,[c] Mercouri G. Kanatzidis[b] and Yanliang Zhang*[a]

[a]Department of Aerospace and Mechanical Engineering, University of Notre Dame, Notre Dame, IN 46556, USA

[b]Department of Chemistry, Northwestern University, Evanston, Illinois 60208, USA

[c]Measurement Sciences Laboratory, Idaho National Laboratory, Idaho Falls, ID 83415, USA

* Corresponding author. *E-mail address:* yzhang45@nd.edu

Abstract

Thermoelectric generators are promising energy sources in remote or harsh environments such as the core of a nuclear reactor where they can power remote sensors and other in-core instrumentation. A high-performance n-type lead telluride material $Pb_{0.975}Ga_{0.025}Te$–0.25%ZnTe was inserted into the core of a nuclear reactor and thermoelectric material properties were continuously monitored while it was irradiated for 228 MW-days to a fast neutron (>1.0 MeV) fluence of 2.0×10^{20} n/cm^2. The electrical conductivity increased within hours of the reactor starting with a peak increase to 343% of the non-irradiated electrical conductivity at the same temperatures. The electrical conductivity subsequently decreased but leveled off at 155-161% of the non-irradiated value near the end of the reactor cycle. The thermoelectric power factor and device power density peaked at 132% of the non-irradiated values within the first few days but fell to 90% of the non-irradiated values around day 9 due to a moderate drop in Seebeck coefficient to 57% of the non-irradiated value. Beyond day 9, the Seebeck coefficient steadily increased until leveling off at 81-85% of its non-irradiated value near the end of the cycle. After the initial transient changes in Seebeck coefficient and electrical conductivity, the power factor of the material in-core was approximately the same as the measured value before irradiation.

However, due to a sudden increase in Seebeck coefficient and electrical conductivity during the last few days, the power factor at the end of the reactor cycle was 8-10% greater than the power factor of the non-irradiated material at the same temperatures. These results indicate that the PbTe based thermoelectric material studied in this work can serve as a solid-state power source for operation in the harsh environment of a nuclear reactor core.

1. Introduction

Nuclear power plants have abundant heat sources which can be harvested with thermoelectric materials to power wireless sensor nodes and other instrumentation, enhancing power plant safety without the need for costly power and data cable installation. The thermoelectric materials could power sensors and instrumentation that are used during both normal power plant operations and loss of power conditions. In the event of a station blackout, the thermoelectric materials can continue to provide power to the sensors and instrumentation, which can, in turn, provide a live feed of data essential for catastrophe mitigation.[1] Radioisotope thermoelectric generators heated by alpha and gamma radiation have been used for decades in deep space exploration where there is insufficient solar irradiance for solar power generation.[2] However, there are few reports on the performance of thermoelectric materials in a nuclear reactor core where there is a high flux of thermal and fast neutron radiation. The in-core irradiation effect on bulk thermoelectric materials like germanium telluride, silicon-germanium, etc. has been studied,[2–6] most under the comparatively low neutron fluences of 10^{13} to 10^{19} n/cm^2. Neutron irradiation at relatively low temperatures (<200°C) created irradiation-induced point defects in these materials, reducing carrier mobility and lowering thermoelectric performance. A thermoelectric generator comprised of bulk nanostructured half-Heusler thermoelectric materials was tested in a reactor core to a fast neutron fluence of 1.5×10^{20} n/cm^2 (>1.0 MeV).[7] Despite a significant decrease in thermoelectric performance due to radiation damage sustained at relatively low temperatures, it was found that the thermoelectric generator can provide stable power in the reactor core if operated at a sufficiently high temperature. The n-type lead telluride material $Pb_{0.975}Ga_{0.025}Te$–0.25%ZnTe studied in this work was exposed to the unprecedented fast neutron fluences of 2.0×10^{20} n/cm^2 (>1.0 MeV) and 4.2×10^{20} n/cm^2 (>0.1 MeV) with a thermal neutron fluence of 1.3×10^{20} n/cm^2 (<1.0 eV).

In recent years, the efficiency of thermoelectric materials has undergone tremendous improvement, especially using the nanostructuring strategy.[8–24] However, apart from the study on the half-Heusler thermoelectric generator mentioned above,[7] advanced nanostructured thermoelectric materials have not been tested in the extreme environment of a nuclear reactor core. Thermoelectric (TE) generators are solid-state devices that convert heat in the form of a temperature gradient into electrical power. Thermoelectric material performance can be increased by increasing the thermoelectric figure of merit, which defined as

$$ZT = \frac{S^2\sigma}{k}T,$$

where S is the Seebeck coefficient, σ is the electrical conductivity, k is the thermal conductivity, and T is the temperature.[25]

Lead telluride is a promising thermoelectric material system for moderate temperature applications due to its high ZT and earth-abundant constituent elements.[19,26–32] The lead telluride material $Pb_{0.975}Ga_{0.025}Te$–0.25%ZnTe was recently shown to have the highest ZT among n-type lead tellurides; this was attributed to the role of Zn which induces nucleation and growth of Ga_2Te_3 in the PbTe matrix, increasing carrier concentration and electrical conductivity while simultaneously lowering thermal conductivity.[19] The same material, hereafter referred to as n-PbTe, was inserted into the core of a 6 MW nuclear research reactor with a core power density of about 70 kW per liter and thermal and fast neutron fluxes of 3.4×10^{13} n/cm^2/s (<1.0 eV) and 6.1×10^{13} n/cm^2/s (>1.0 MeV), respectively, while under operation at the nominal 5.7 MW. The Seebeck coefficient, electrical conductivity, power factor, and thermoelectric power output were monitored continuously while the material was irradiated at full reactor power for 39 days. Within the first 5 days, the in-core irradiation caused a surprising increase in electrical conductivity to more than three times the conductivity of the non-irradiated material at the same temperatures. Meanwhile, the Seebeck coefficient decreased moderately. Shortly after

hitting their maximum and minimum on days 4.6 and 8.0, respectively, the electrical conductivity began to decrease and Seebeck coefficient began to increase until leveling off at 155% and 81% of their non-irradiated properties evaluated at the same temperatures. The combination of increased electrical conductivity and moderately decreased Seebeck coefficient resulted in a thermoelectric power factor that was approximately the same as the non-irradiated value for most of the reactor cycle. However, three days before the end of the experiment, the nuclear reactor was shut down for routine maintenance. Upon restarting to the same temperatures, the Seebeck coefficient and thermal conductivity suddenly increased to 161% and 85% of their non-irradiated values, respectively. This resulted in a power factor that was 108-110% of the non-irradiated power factor at the end of the experiment.

2. Experimental

The thermoelectric properties of the n-PbTe bar that was inserted into the reactor were measured before irradiation (shown in Fig. 1). To investigate the thermal stability of the material prior to the in-core test, the bar was thermally cycled to 450°C three times. The thermoelectric properties were measured upon heating and cooling during each thermal cycle. Electrical conductivity and Seebeck coefficient changed by ~3% (less than the measurement uncertainty) between the first and second trials, and no changes were observed between the second and third cycle. To simulate the relatively extreme thermal conditions the bar may experience in the reactor (such as rapid heating or cooling, as well as the potential of exceeding the material's preferred maximum hot side temperature of 450°C) the bar was rapidly thermally cycled between 150°C and 480°C for 9 hours, followed by three additional thermal cycles with measurements upon heating and cooling. The rapid thermal cycles to 480°C caused the Seebeck coefficient to decrease moderately while electrical conductivity increased, but no further changes were observed after additional thermal cycling. These results indicate that if the bar

remains below 480°C in the reactor (as was later confirmed), any changes in material properties must not be due to temperature effects, but to the effects of irradiation. The values plotted in Fig. 1 are the averages of the last two thermal cycles. Additional details about the material synthesis and measurements can be found in the Methods section.

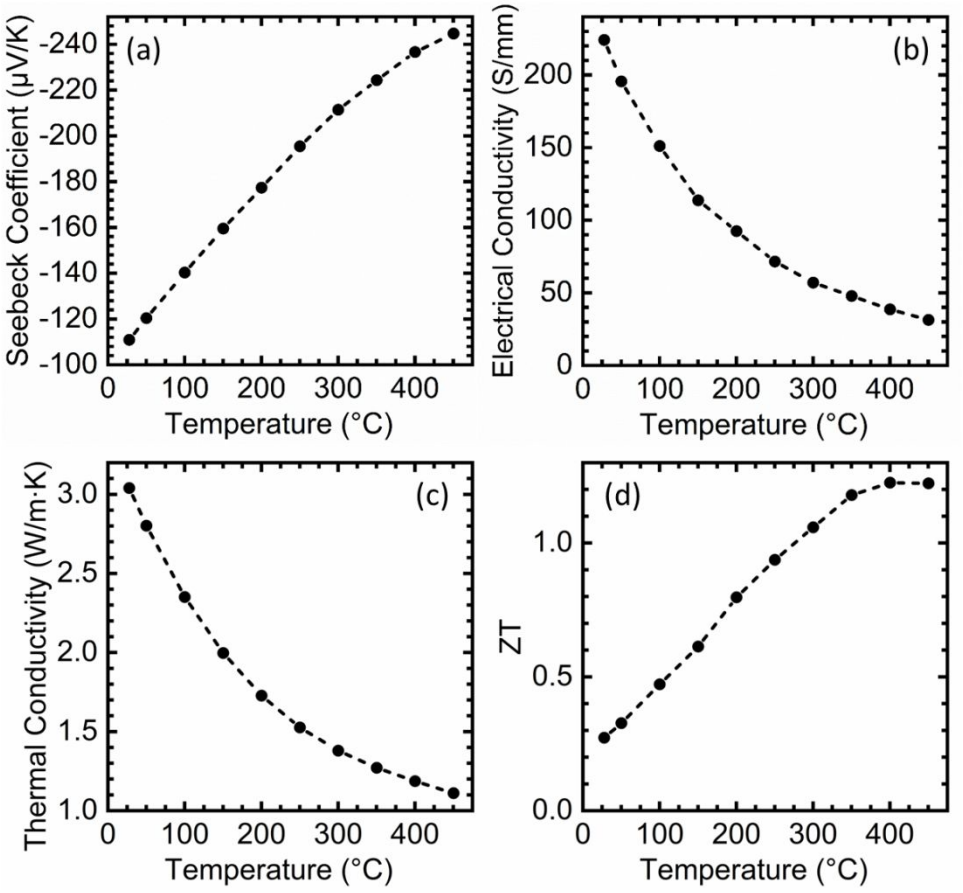

Fig. 1 Thermoelectric property measurements of the n-PbTe bar ($Pb_{0.975}Ga_{0.025}Te$–0.25%ZnTe) before it was inserted into the nuclear reactor showing (a) Seebeck coefficient, (b) electrical conductivity, (c) thermal conductivity, and (d) thermoelectric figure of merit ZT.

In section 3.1, these temperature-dependent material properties of the bar before irradiation are plotted alongside the properties of the bar in the reactor core to reveal the irradiation effect on material properties in-situ.

The aluminum test capsule shown in Fig. 2 was designed and constructed to house the n-PbTe TE bar in the center of the nuclear reactor core.

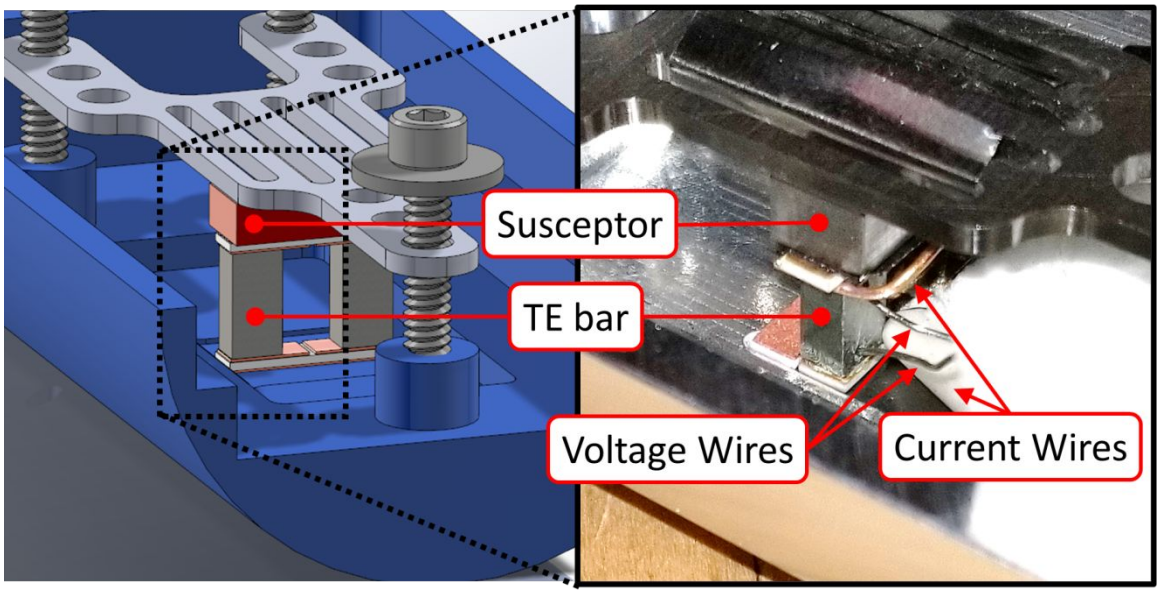

Fig. 2 3D model (left) and photograph (right) showing the n-PbTe thermoelectric (TE) bar held inside the test capsule. In the 3D model, the susceptor is shown in red and the housing of the aluminum test capsule is shown in blue.

While only one TE bar was measured in the reactor, a second TE bar was included in the test capsule to provide mechanical support and prevent excess strain on the bar that was measured. The hot side of the TE bar was heated using a tungsten susceptor which interacts with the abundant gamma rays in the reactor core to generate heat. The test capsule was placed in a titanium tube (not shown in Fig. 2) inside the reactor core which was surrounded by the reactor pool water. A controllable flow of cooling gas passed between the inside of the titanium tube and the outside of the aluminum test capsule, allowing precise control over the TE bar cold side temperature. To electrically isolate the TE bar from the test capsule, the bar was soldered to Direct Bond Copper (DBC) pieces. Copper wires, which were previously welded to the DBC pieces, allow current to be sent through the sample for electrical resistance measurements. Two small divots ~100 μm deep were carefully drilled into the TE bar, as shown in the photograph in Fig. 2, and the wires used to measure voltage were inserted into the divots during assembly (the divots provided mechanical stabilization to ensure the wires remained in contact with the sample during loading into the reactor). The Seebeck voltage was measured by the same voltage

probes used for resistivity measurements, while the temperature at those locations was determined from the measured thermal resistance between the thermocouples and the voltage probes. Additional details about the in-situ measurements can be found in the Methods section.

3. Results and discussion

3.1 In-core thermoelectric material performance

Shown in Fig. 3 are the in-situ measurement results of the n-PbTe bar while it was in the reactor, including the hot- and cold-side temperatures, electrical conductivity, Seebeck coefficient, and power factor.

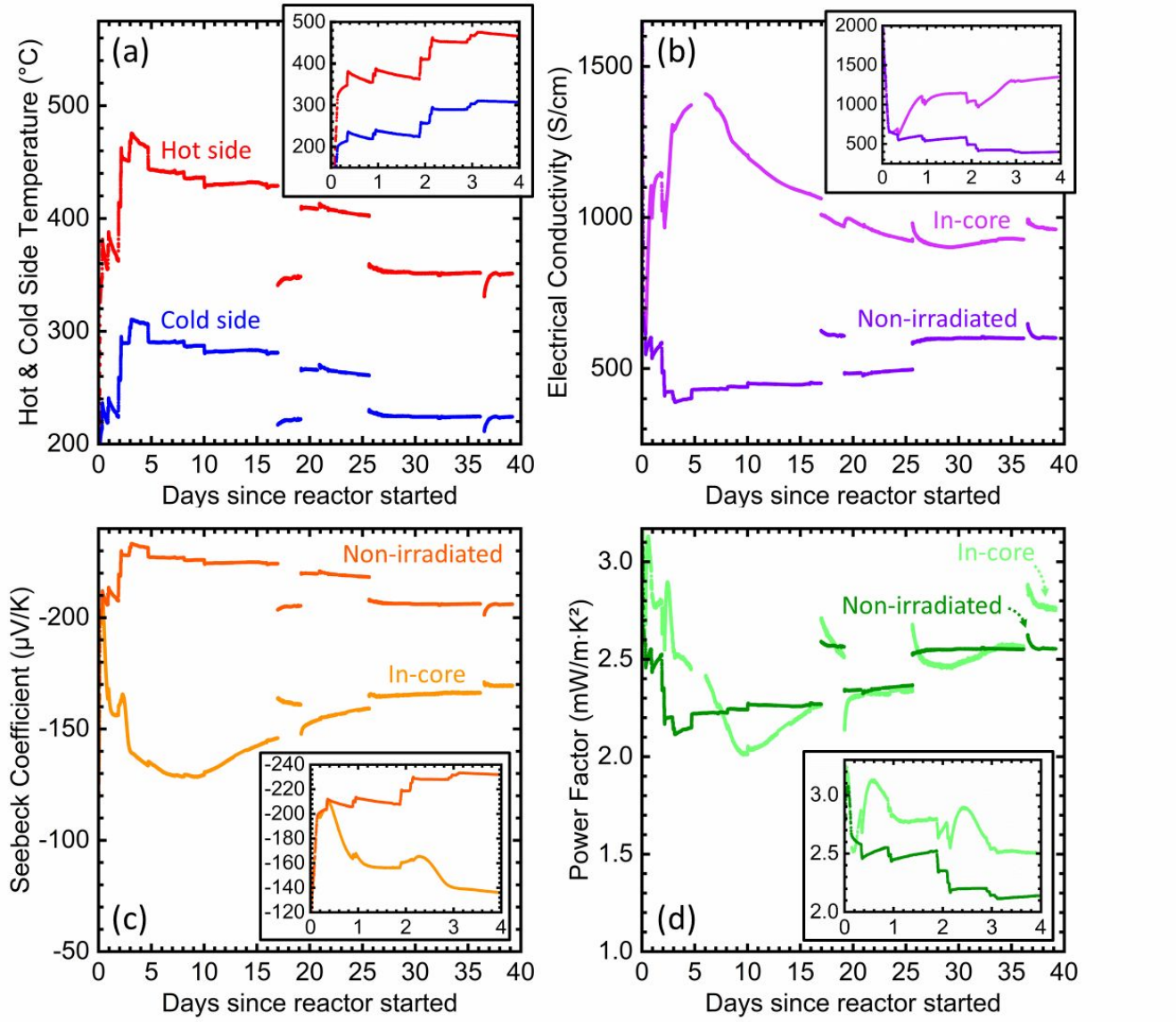

Fig. 3 In-core measurement results of the n-PbTe TE bar showing (a) the hot- and cold-side temperatures, (b) electrical conductivity, (c) Seebeck coefficient, and (d) power factor. Each figure contains an inset showing a close-up of the data during the first four days. Figures (b)-(d) include the corresponding non-irradiated material properties of the same bar measured before irradiation, presented at the same temperatures as the bar in the reactor.

The reactor was brought to full power (5.7 MW) during the first 3.5 hours. The subsequent step-like increases in temperature shown in the inset of Fig. 3(a) during the first four days are due to changes in the cooling gas flowrate. The reactor was shut down on day 17 and upon startup the cooling gas flow rate was increased, resulting in relatively lower temperatures from days 17-19. The sudden increase and decrease in temperatures on days 19 and 25.5, respectively, were due to further changes in the cooling gas flow rate. The transient spike in temperatures on day 36.5 was due to a sudden reactor shutdown and startup for reactor maintenance (some transient data is omitted from Fig. 3).

Within hours of reaching full reactor power, the electrical conductivity of the n-PbTe started to increase. It continued to increase until day 4.6 when it reached its maximum of 343% of the electrical conductivity before irradiation. All pre-irradiation values referred to herein, as well as the non-irradiated data presented in Fig. 3, are the integral average of the measurement data of the bar before insertion into the reactor core (Fig. 1), evaluated at the actual temperatures of the bar in the reactor core. In other words, the time- and temperature-dependent non-irradiated electrical conductivity plotted in Fig. 3(b) was calculated at every discrete moment in time as

$$\sigma_{non-irr}(T,t) = \int_{T_c(t)}^{T_h(t)} \sigma(T)dT/\big(T_h(t) - T_c(t)\big),$$

where $\sigma(T)$ is the temperature-dependent electrical conductivity measured before irradiation (shown in Fig. 1), and $T_h(t)$ and $T_c(t)$ are the hot- and cold-side temperatures, respectively, of the bar inside the reactor at any given moment in time t along the abscissa of Fig. 3. The time- and temperature-dependent Seebeck coefficient of the non-irradiated bar plotted in Fig. 3(c) was calculated analogously. Meanwhile, Seebeck coefficient decreased and hit its low of 57% of

the non-irradiated value on day 8.0. The initial increase in conductivity more than offset the decrease in Seebeck coefficient and the net result was an increase in power factor relative to the non-irradiated property through day 7.6.

Soon after hitting its minimum on day 8.0, Seebeck coefficient began to recover despite constant temperatures and unchanging reactor power and flux; meanwhile, electrical conductivity steadily decreased. Despite this decrease, electrical conductivity remained well above the non-irradiated value for the remainder of the reactor cycle. The increasing Seebeck coefficient and decreasing electrical conductivity resulted in the minimum measured power factor and power density (Fig. 4) of 90% of the non-irradiated values on day 9.6.

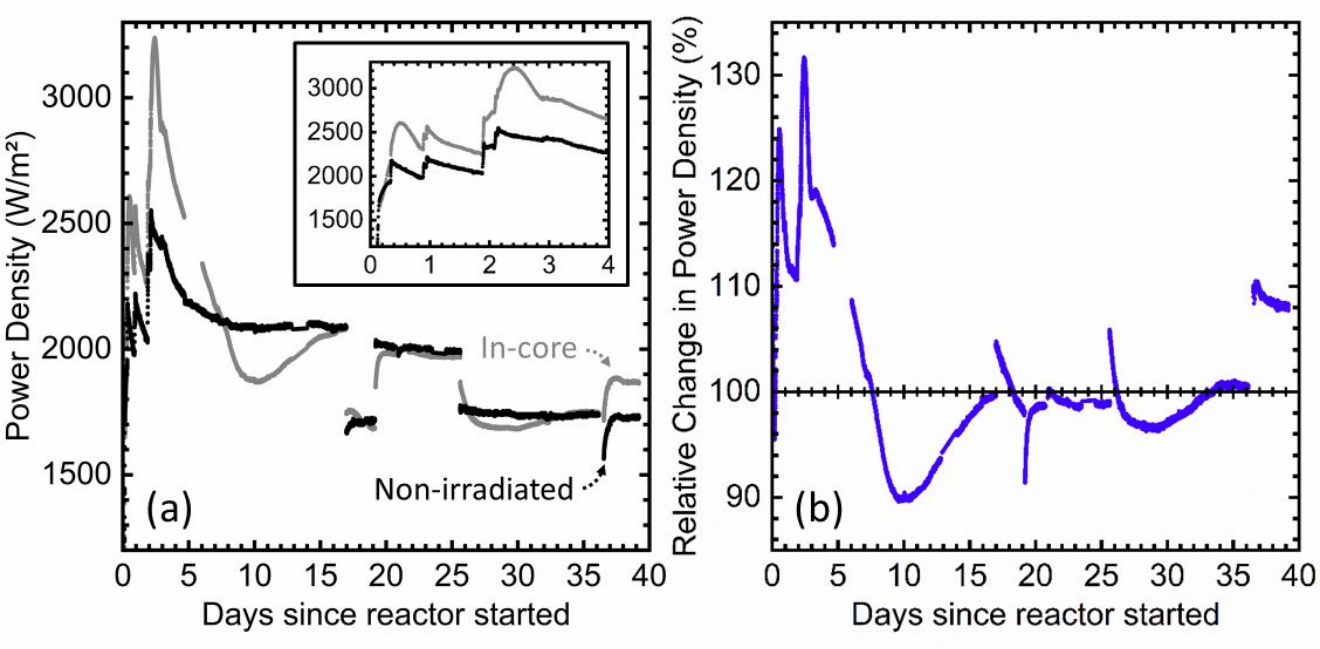

Fig. 4 (a) In-core power density of the n-PbTe material along with the power density of the bar before irradiation at the same temperatures and (b) the relative change in power density, which is the ratio of the in-core and non-irradiated power density.

The rate of decrease of electrical conductivity began to wane around day 9 while Seebeck coefficient continued to recover steadily. The resulting power density and power factor were, on average, 99.3% of the non-irradiated values from day 17 through 36 just before the last reactor shutdown and subsequent startup due to scheduled maintenance. Despite returning to the same

temperatures and reactor power, both Seebeck coefficient and electrical conductivity suddenly increased on day 36 after the reactor started back up, resulting in an in-situ power factor as high as 110% of the non-irradiated value.

3.2 Causes for material property changes

Consider the relaxation time model in which the Seebeck coefficient is described by

$$S = \frac{\pi^2 k_B^2 T}{3e(\xi_F - E_c)}\left(\frac{3}{2} + r\right), \quad (1)$$

where k_B is the Boltzmann constant, T is the temperature, e is carrier charge, ξ_F is the Fermi level, E_c is the conduction band edge, and r is the index of relaxation time related to the kinetic energy of the charge carrier.[33] The index r ranges from $-1/2$ for purely thermal scattering to $3/2$ for electron scattering by ionized impurities. Substituting the Fermi level for metals,[34]

$$\xi_F - E_c = \frac{h^2}{8m^*}\left(\frac{3n}{\pi}\right)^{2/3}, \quad (2)$$

where h is the Planck constant, m^* is the charge carrier effective mass, and n is the carrier concentration, into equation (1) yields

$$S = \frac{8\pi^2 k_B^2 m^* T}{3eh^2}\left(\frac{\pi}{3n}\right)^{2/3}\left(\frac{3}{2} + r\right). \quad (3)$$

Equation (3) is often used with the rightmost term omitted (with $r = -1/2$, assuming energy-independent scattering) to estimate the Seebeck coefficient for semiconductors with high levels of doping;[12,13,35–37] this form makes clear that the Seebeck coefficient is not necessarily dominated by the carrier concentration in a given material system. The electrical conductivity of the system is described by

$$\sigma = ne\mu = \frac{ne^2\tau}{m^*}, \quad (4)$$

where μ is the charge carrier mobility and τ is the charge carrier relaxation time.[34]

Equations (3) and (4) indicate that a decrease in m^* or an increase in τ or n must occur to result in the increased σ and decreased S observed in the reactor. An increase in τ is unlikely because neutron irradiation generates point defects that scatter charge carriers and decrease τ. A change in m^* substantial enough to cause the significant changes in thermoelectric properties witnessed in the reactor is also unlikely because such a large change in m^* would require dramatic changes to the electronic band structure of the material, which, in turn requires considerable changes to the material crystal structure and/or composition. These physical considerations and the experimental data from the nuclear reactor indicate the changes in thermoelectric properties are due primarily to changes in carrier concentration. The n-PbTe material contains nanoscale Ga_2Te_3 precipitates which cause some Te deficiency in the PbTe matrix of the native, non-irradiated material;[19] however, not all the Ga is contained within the nanoprecipitates – there is a uniform distribution of Ga throughout the material. Meanwhile, neutrons in the reactor have sufficient energy to split PbTe into elemental Pb and Te, which would allow the formation of new Ga_2Te_3 precipitates and/or growth of existing Ga_2Te_3 precipitates. The effect would be a further increase in Te deficiency in the PbTe matrix and thus increased carrier concentration. Just as was seen during the first several days in the reactor core, the result is an increase in electrical conductivity σ and a decrease in Seebeck coefficient S.

Now, beginning on day 4.6, electrical conductivity began to drop while Seebeck coefficient began to increase on day 8.0. Neither a decrease in carrier concentration nor an increase in electron effective mass alone can justify why these properties reversed trend at distinctly different times. Instead, these trends are expected to be the result of irradiation-induced defects such as vacancies and interstitials. These defects cause mass and strain fluctuations in the crystal lattice, lowering charge carrier mobility μ and decreasing electrical conductivity. In the case of Seebeck coefficient, these point defects can effectively transition the dominant charge

carrier scattering mechanism from primarily acoustic phonon scattering ($r = -1/2$) to a mix of phonon and ionized impurity scattering with $-1/2 < r < 3/2$. By equation (4), the result is an increase in Seebeck coefficient. In summary, the changes in material properties during the first week in the reactor were due primarily to an increase in the material carrier concentration. Changes in carrier concentration appear to have leveled off between days 5 to 9, and subsequent material property changes are attributed to irradiation-induced defects.

4. Conclusions

The high-performing n-type lead telluride composition $(Pb_{0.975}Ga_{0.025}Te)_{0.9975}$-$(ZnTe)_{0.0025}$ was inserted into the core of a 6 MW nuclear reactor and irradiated at full reactor power for 39 days. The electrical conductivity increased significantly for the entirety of the reactor cycle, with a peak increase to 343% of the non-irradiated value on day 4.6 followed by a steady decrease to 155-161% of the non-irradiated value during the last two weeks of the reactor cycle. Seebeck coefficient decreased to a minimum of 57% of the non-irradiated value on day 8 followed by a partial recovery until it leveled off at 81-85% of the non-irradiated value for the remainder of the reactor cycle. After the initial transients during the first two weeks, the power factor of the irradiated material was approximately the same as that of the material before irradiation at the same temperatures; however, the power factor increased during the last few days to 108-110% of the power factor of the non-irradiated material. It is expected that the neutron irradiation triggered an increase in carrier concentration due to an increase in the density of Ga_2Te_3 nanoprecipitates and resulting Te deficiency in the PbTe matrix. The increased carrier concentration caused a significant increase in electrical conductivity as well as a decrease in Seebeck coefficient. Measurement results indicate that changes in carrier concentration were minimal beyond day 9 and the subsequent decrease in electrical conductivity and increase in Seebeck coefficient were due primarily to irradiation-induced point defects and associated

charge carrier scattering. These findings suggest that – despite significant irradiation-induced changes to the microstructure – the n-type lead telluride material system studied herein can maintain very similar thermoelectric performance as the non-irradiated material while in the core of a nuclear reactor. In combination with studies on the effect of irradiation on thermal conductivity, these findings may guide thermoelectric material property optimization in new and unexpected ways.

5. Materials and methods

5.1 Thermoelectric material synthesis

High-purity Pb wire (99.99%, American Elements, USA), Te shot (99.999%, 5 N Plus, Canada), Zn shot (99.999%, Sigma-Aldrich, USA), and Ga shots (99.99%, Sigma-Aldrich, USA) were weighed and mixed in stoichiometric proportions. The total mass of the sample was 15 g. Then, the stoichiometric mixture of elements was sealed in an evacuated quartz tube (the inner diameter was 10 mm and the thickness of its walls was 1.5 mm) and heated slowly to 1373 K at a rate of 100 K/h, kept at this temperature for 6 h, then quenched in cold water to room temperature. The obtained ingot was crushed, hand-ground into a fine powder, and sintered by spark plasma sintering (SPS) at 773 K under a pressure of 40 MPa in vacuum for 5 min to obtain densified bulk sample of 12.7 mm diameter and 12 mm height. The SPS'd bulk sample was then heated to 723 K at a rate of 100 K/h, annealed under vacuum at this temperature for 24 h, and subsequently slowly cooled down to room temperature.

5.2 Thermoelectric material property measurement before irradiation

Seebeck coefficient and electrical conductivity were measured simultaneously with a ZEM-3 (Ulvac Riko, Inc.). The thermal conductivity was calculated as $k = \alpha\rho c_p$, where α is the thermal diffusivity measured with the laser flash method (Netzsch LFA 457), ρ is the density which was measured directly, and c_p is the specific heat, which was calculated by the Dulong-Petit law.

5.3 In-situ measurements in the nuclear reactor

A current source and nanovoltmeter (Keithley 6221 and 2182A) measured the TEG electrical resistance. The peak thermoelectric power was calculated as $P_{\max} = V_{\mathrm{oc}}^2/4R$, where V_{oc} is the open-circuit voltage and R is the electrical resistance. The Seebeck voltage was monitored continuously with a programmable multimeter (Agilent 34970A).

CRediT authorship contribution statement

Nicholas Kempf: Conceptualization, Methodology, Formal analysis, Investigation, Writing – Original Draft, Writing – Review & Editing, Visualization, Supervision, Project administration. **Zhong-Zhen Luo:** Investigation. **Hongyao Xie:** Investigation. **Joshua Daw:** Resources. **Mercouri G. Kanatzidis:** Supervision, Writing – Review & Editing. **Yanliang Zhang:** Conceptualization, Writing – Review & Editing, Supervision, Project administration, Funding acquisition.

Conflicts of interest

There are no conflicts of interest to declare.

Acknowledgments

This work was funded by the U.S. Department of Energy, Office of Nuclear Energy, under Award DE-NE0008812.

References

1 D. A. Clayton, W. H. J. Andrews and R. Lenarduzzi, *ORNL, Rep. No. ORNL/TM-2012/442*, 2012, 442.

2 H. Wang and K. J. Leonard, *Appl. Phys. Lett.*, 2017, **111**, 1–5.

3 J. C. Danko, G. R. Kilp and P. V. Mitchell, *Adv. Energy Convers.*, , DOI:10.1016/0365-1789(62)90011-5.

4 J. W. Vandersande, J. McCormack, A. Zoltan and J. Farmer, in *Proceedings of the Intersociety Energy Conversion Engineering Conference*, 1990.

5 M. Idnurm and K. Landecker, *Br. J. Appl. Phys.*, , DOI:10.1088/0508-3443/18/8/422.

6 Y. Li, J. Li, J. Du, J. Han, Q. Xiang and C. Zhang, *J. Nucl. Mater.*, 2020, **528**, 151856.

7 N. Kempf, M. Saeidi-Javash, H. Xu, S. Cheng, M. Dubey, Y. Wu, J. Daw, J. Li and Y. Zhang, *Energy Convers. Manag.*, , DOI:10.1016/J.ENCONMAN.2022.115949.

8 L. D. Zhao, V. P. Dravid and M. G. Kanatzidis, *Energy Environ. Sci.*, 2014, **7**, 251–268.

9 Y. Zheng, T. J. Slade, L. Hu, X. Y. Tan, Y. Luo, Z. Z. Luo, J. Xu, Q. Yan and M. G. Kanatzidis, *Chem. Soc. Rev.*, 2021, **50**, 9022–9054.

10 H. T. Liu, Q. Sun, Y. Zhong, Q. Deng, L. Gan, F. L. Lv, X. L. Shi, Z. G. Chen and R. Ang, *Nano Energy*, 2022, **91**, 106706.

11 C. Jung, B. Dutta, P. Dey, S. jae Jeon, S. Han, H. M. Lee, J. S. Park, S. H. Yi and P. P. Choi, *Nano Energy*, 2021, **80**, 105518.

12 K. B. Spooner, A. M. Ganose and D. O. Scanlon, *J. Mater. Chem. A*, 2020, **8**, 11948–11957.

13 S. N. Guin, D. S. Negi, R. Datta and K. Biswas, *J. Mater. Chem. A*, 2014, **2**, 4324–4331.

14 A. Bhardwaj, N. S. Chauhan and D. K. Misra, *J. Mater. Chem. A*, 2015, **3**, 10777–10786.

15 Y. Zhu, J. Carrete, Q. L. Meng, Z. Huang, N. Mingo, P. Jiang and X. Bao, *J. Mater. Chem. A*, 2018, **6**, 7959–7966.

16 D. K. Misra, A. Bhardwaj and S. Singh, *J. Mater. Chem. A*, 2014, **2**, 11913–11921.

17 N. Jia, X. Y. Tan, J. Xu, Q. Yan and M. G. Kanatzidis, *Accounts Mater. Res.*, 2022, **3**, 237–246.

18 Y. Xiao, H. Wu, H. Shi, L. Xu, Y. Zhu, Y. Qin, G. Peng, Y. Zhang, Z. H. Ge, X. Ding and L. D. Zhao, *Adv. Energy Mater.*, , DOI:10.1002/aenm.202200204.

19 Z.-Z. Luo, S. Cai, S. Hao, T. P. Bailey, Y. Luo, W. Luo, Y. Yu, C. Uher, C. Wolverton, V. P. Dravid, Z. Zou, Q. Yan and M. G. Kanatzidis, *Energy Environ. Sci.*, 2022, **15**, 368–375.

20 S. Chen, K. C. Lukas, W. Liu, C. P. Opeil, G. Chen and Z. Ren, *Adv. Energy Mater.*, 2013, **3**, 1210–1214.

21 L. D. Zhao, S. H. Lo, Y. Zhang, H. Sun, G. Tan, C. Uher, C. Wolverton, V. P. Dravid and M. G. Kanatzidis, *Nature*, 2014, **508**, 373–377.

22 C. Zhou, Y. K. Lee, Y. Yu, S. Byun, Z. Z. Luo, H. Lee, B. Ge, Y. L. Lee, X. Chen, J. Y. Lee, O. Cojocaru-Mirédin, H. Chang, J. Im, S. P. Cho, M. Wuttig, V. P. Dravid, M. G. Kanatzidis and I. Chung, *Nat. Mater.*, 2021, **20**, 1378–1384.

23 B. Jiang, Y. Yu, J. Cui, X. Liu, L. Xie, J. Liao, Q. Zhang, Y. Huang, S. Ning, B. Jia, B. Zhu, S. Bai, L. Chen, S. J. Pennycook and J. He, *Science (80-.).*, 2021, **371**, 830–834.

24 B. Zhu, X. Liu, Q. Wang, Y. Qiu, Z. Shu, Z. Guo, Y. Tong, J. Cui, M. Gu and J. He, *Energy Environ. Sci.*, 2020, **13**, 2106–2114.

25 D. M. Rowe, *Thermoelectrics Handbook: Macro to Nano*, CRC Press, 2005.

26 Z. Z. Luo, S. Cai, S. Hao, T. P. Bailey, I. Spanopoulos, Y. Luo, J. Xu, C. Uher, C. Wolverton, V. P. Dravid, Q. Yan and M. G. Kanatzidis, *Angew. Chemie - Int. Ed.*, 2021, **60**, 268–273.

27 D. Wang, Y. Qin, S. Wang, Y. Qiu, D. Ren, Y. Xiao and L. D. Zhao, *Ann. Phys.*, 2020, **532**, 1–8.

28 B. Qin, X. Hu, Y. Zhang, H. Wu, S. J. Pennycook and L. D. Zhao, *Adv. Electron. Mater.*, 2019, **5**, 1–8.

29 Y. Xiao, H. Wu, D. Wang, C. Niu, Y. Pei, Y. Zhang, I. Spanopoulos, I. T. Witting, X. Li, S. J. Pennycook, G. J. Snyder, M. G. Kanatzidis and L. D. Zhao, *Adv. Energy Mater.*, 2019, **9**, 1–11.

30 J. Zhang, D. Wu, D. He, D. Feng, M. Yin, X. Qin and J. He, *Adv. Mater.*, 2017, **29**, 1–7.

31 C. Zhu, J. Zhang, H. Ming, L. Huang, Y. Li, T. Chen, D. Li, B. Zhang, J. Xu and X. Qin, *J. Mater.*, 2021, **7**, 146–155.

32 C. Zhu, J. Zhang, H. Ming, X. Lou, L. Huang, T. Chen, B. Zhang, D. Li, H. Xin and X. Qin, *Appl. Phys. Lett.*, , DOI:10.1063/5.0013039.

355 33 F. D. Rosi, *Solid State Electron.*, 1968, **11**, 833–868.

356 34 C. Kittel and D. F. Holcomb, *Introduction to Solid State Physics*, 1967, vol. 35.

357 35 G. J. Snyder and E. S. Toberer, *Nat. Mater.*, 2008, **7**, 105–114.

358 36 S. Chen and Z. Ren, *Mater. Today*, 2013, **16**, 387–395.

359 37 Z. G. Chen, G. Hana, L. Yanga, L. Cheng and J. Zou, *Prog. Nat. Sci. Mater. Int.*, 2012, **22**, 535–

360 549.

361